Effects of impurity mixing on α-heating in two-temperature hot dense deuterium-tritium plasmas

Xing-Yu Li(李星宇)[1], Bin He(何斌)[1,*], Yong Wu(吴勇)[1,†]
Hua-Yun Shen(沈华韵)[1], and Jian-Guo Wang(王建国)[1]
[1]Institute of Applied Physics and Computational Mathematics, Beijing 100094, China

September 9, 2026

Abstract

The mixing of impurities with deuterium-tritium (DT) fuel affects the energy deposition of α particles in inertial confinement fusion (ICF). This study investigates how impurity mixing influences energy partition during α-heating when the ion temperature (T_i) exceeds the electron temperature (T_e). Two kinds of impurity ions, beryllium (Be) and gold (Au), are considered. We conduct calculations at mixture densities of 4.15 and 415.0 g/cm^3, with T_e ranging from 0.1 to 100.0 keV. The average ionization degree and partial density of each ion species are obtained through the average atom model. Results show that when the number ratio of impurity ions to DT ions (R) reaches 0.05, the mixing of Be significantly reduces the energy partition fraction of DT ions (η_DT). In the case of Au mixing, it occurs at $R = 0.01$. At fixed T_e and R, the reduction in η_DT grows slowly with T_i, while the energy partition to electrons remains independent of T_i. Meanwhile, the heating of both impurity ions is easier than that of DT ions, with Au ions being heated faster than Be ions. The different effects caused by the two impurities primarily originate from their distinct charge states and masses. Our work quantitatively analyzes the influence of realistic two-temperature plasma conditions on impurity mixing effects. The findings provide references for impurity tolerance and shell material selection in ICF target design.

Keywords: α-heating, deuterium-tritium plasma, two-temperature plasma, mixture
PACS: 52.20.Hv, 52.58.Ei, 52.25.Fi, 52.50.Gj

1. Introduction

The process of α-heating, whereby fusion-born 3.54 MeV α particles deposit their energy into the deuterium-tritium (DT) fuel, is fundamental for maintaining self-sustained plasma burning in inertial confinement fusion (ICF) [1,2]. A quantitative understanding of α-heating is essential for the modeling of ICF, which requires precisely calculating the stopping power of α particles in the medium. Numerous theoretical frameworks have been proposed on this issue over the past century. In general, they can be divided into two categories. One

*Corresponding author. E-mail: hebin-rc@163.com
†Corresponding author. E-mail: wu_yong@iapcm.ac.cn

is based on the binary collision theory, and the other employs dielectric functions. Within the binary collision framework, early models mainly adopted classical mechanics [3–5], while the development of quantum mechanical methods further incorporated inelastic collision processes [6–10]. The dielectric approach was originally introduced by Lindhard for describing stopping powers in the electron gas [11]. Later developments based on it have also branched into classical [12] and quantum [2,13] formulations. In recent models, methods such as the generalized Fokker-Planck equation [14] and dimensional continuation [15] have been introduced into the calculation of stopping powers.

In the ignition target design of indirect-drive ICF, materials with low atomic number (Z) such as carbon-hydrogen (CH), beryllium (Be) and polyimide are often used as ablators. Especially, Be shells have merits like lower albedo and higher mass density, which make them absorb energy more efficiently and have better tolerance to ice-layer roughness during the ablation [16]. Meanwhile, to limit radiative losses from the fuel and enhance inertia for delaying disassembly, high-Z materials such as gold (Au) and tungsten (W) are utilized in the double-shell ignition target design [17]. Impurities from the ablator or shell materials inevitably mix into the central DT fuel because of hydrodynamic instabilities such as the Rayleigh-Taylor instability during the implosion, or due to the use of chemical compounds containing hydrogen isotopes [18]. This mixing can significantly degrade performance by absorbing energy from α particles, reducing ion heating, neutron yield, and target gain, while increasing the ignition energy [18,19]. Utilizing the widely-used model proposed by Brown, Preston, and Singleton Jr (BPS) [15], prior work [20,21] examined the influence of Be and uranium (U) mixed with DT on the transport of α particles. They reported that both the range of the projectile and the energy deposition in electrons exhibit an inverse correlation with the density and Z of the impurity particles. Our recent study [22] investigated the electron-ion energy partition fraction during α-heating in the DT fuel mixed with Au ions, which finds that Au impurity can drastically reduce the energy allocated to DT ions and enhance the range of α particles. The authors proposed that the BPS model is invalid in this case, since the high charge state of Au ions leads to a strong coupling with projectiles, while the BPS model employs the perturbation method to deal with weakly coupled plasmas.

During the process of actual ICF implosions, electron-ion temperature non-equilibrium arises due to unequal α particle energy deposition caused by their different masses, in combination with energy losses from bremsstrahlung radiation and electron heat conduction. In the self-heating stage after ignition, ions experience higher energy deposition and have less energy loss than electrons, which leads to ion temperature exceeding electron temperature [23]. The increase in ion temperature enhances the fusion reaction rate, which produces more α particles and forms a positive feedback. In a series of experiments conducted on the OMEGA facility [24], the ratio of average ion temperature to average electron temperature in ICF implosions can reach about 2.56 to 4.21.

To our knowledge, analyses of impurity mixing effects on α-heating have predominantly focused on scenarios with equal electron and ion temperatures. Owing to the mass differences among impurity ions, DT ions, and electrons, the energy deposition of α particles differs across various plasma compositions. Furthermore, since the stopping power of α particles in a given composition is strongly affected by its temperature, it follows qualitatively that two-temperature conditions will alter the effect of impurities on α-heating. Therefore, investigating the energy deposition of α particles in two-temperature mixed plasmas is of significant importance, which is

the primary motivation of the present study. While our previous work [22] has examined Au mixing in DT fuel under equal electron and ion temperatures, here we are concerned with non-equal temperature conditions. Our research can provide a quantitative understanding of how different types of impurities affect energy partition in α-heating under various ion and electron temperature conditions. The results can serve as a reference for impurity tolerance and shell material selection in ICF target design. In this study, we take Be and Au ions, respectively, as representative low-Z and high-Z impurities, which are separately considered in mixture with the DT fuel. A comparative investigation of these two elements helps us enhance the overall understanding of impurity mixing effects on α-heating.

This paper is structured as follows. Section 2 will discuss the average ionization degree and the partial density of each ion component in the mixtures under equilibrium conditions. In Section 3, we will briefly introduce the methods for calculating the stopping powers and their key properties. Section 4 will present the derived electron-ion energy partition fractions in α-heating, analyzing their trends and underlying physical mechanisms. Section 5 will summarize the conclusions. For simplicity, D and T ions are treated as a single ion species with equal numbers of each in this work (referred to as DT ions), yielding an effective mass number of ~ 2.5. The density of the mixture ($\rho_{\rm mix}$) is set to 4.15 and 415.0 g/cm^3, which corresponds to the ion number density of 10^{24} and 10^{26} cm^{-3} in pure DT plasmas, respectively. The electron temperature ranges from 0.1 to 100.0 keV. According to particle-in-cell simulation results of the National Ignition Facility (NIF) capsule implosions [25], high-density ($\sim 10^{26}$ cm^{-3}) regions appear at the edge of the hot spot during the compression and ignition/burn stages, while low-density ($\sim 10^{24}$ cm^{-3}) conditions are observed in the expansion stage. After ignition, the center of the hot spot can reach temperatures near 100.0 keV. The low-temperature (~ 0.1 keV) environment corresponds to the hot spot periphery during the compression stage. All projectiles are α particles.

2. Plasma States in the Mixtures

The stopping power of α particles depends on the states of the mixed plasmas. Due to the sufficiently short relaxation time of the investigated dense plasmas, we consider the electron component to be in thermal equilibrium at the temperature $T_{\rm e}$ [22]. Furthermore, all ion species including DT and impurity ions are simply assumed to be in equilibrium at a common ion temperature $T_{\rm i}$. In ICF plasmas, the ion temperature often exceeds that of electrons ($T_{\rm i} > T_{\rm e}$). In the following calculations, we fix $T_{\rm e}$ at selected values within the range of 0.1 to 100.0 keV, and for each we choose a series of $T_{\rm i}$ above $T_{\rm e}$ but not exceeding 100.0 keV, so as to more clearly identify the trends of impurity mixing effects under varying two-temperature conditions. DT ions are taken as fully ionized over the temperature range of 0.1-100.0 keV, which corresponds to an average ionization degree of 1.0. For impurity ions, their average ionization degrees are calculated through the Hartree-Fock-Slater approach based on the average atom model [26]. The derived average ionization degrees of Be ($< Z_{\rm Be} >$) and Au ($< Z_{\rm Au} >$) are shown in Figure 1. For Be ions, the ionization degree is ~ 3.4 when $\rho_{\rm Be} = 4.15$ g/cm^3 and $T_{\rm e} = 0.1$ keV, and it becomes close to 4.0 under other conditions. This signature suggests that Be ions are almost fully ionized over the studied temperature range. In contrast, $< Z_{\rm Au} >$ rises rapidly between 0.1-5.0 keV and approaches 79.0 at higher temperatures, which indicates the presence of bound electrons when $T_{\rm e}$ is low. At the density of 415.0 g/cm^3 and low temperatures, $< Z_{\rm Be} >$ and $< Z_{\rm Au} >$ can exceed their corresponding values at 4.15 g/cm^3, which may be attributed to the pressure ionization [27].

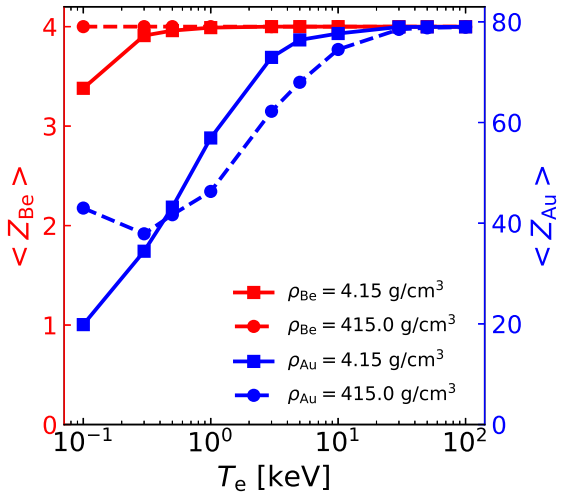


Fig. 1. Average ionization degrees of Be ($< Z_{\rm Be} >$, the red curves) and Au ($< Z_{\rm Au} >$, the blue curves) ions varying with the electron temperature $T_{\rm e}$, calculated from the average atom model. The solid curves with squares and the dashed curves with circles mark the results when densities of Be ($\rho_{\rm Be}$) and Au ($\rho_{\rm Au}$) are equal to 4.15 g/cm^3 and 415.0 g/cm^3, respectively.

Here we discuss the composition of the plasma mixture under equilibrium conditions. Following prior work [22], the partial density of an ionic species s (ρ_s) can be defined as the ratio of its mass to the volume it occupies within the mixture. Besides, the total density ($\rho_{{\rm mix}-s}$) is defined as the mass divided by the total volume of the mixture. Correspondingly, one can define the partial and total number densities (n_s and $n_{{\rm mix}-s}$) for species s. The degree of mixing R is given by the total number density of impurity ions relative to that of DT ions, which also equals the corresponding ratio of their particle numbers in the mixture. Generally, the number of hot impurity ions entering the DT fuel region is expected to be much smaller than that of DT ions. Using measured data including X-ray emission, neutron yield, and hot spot temperature, Ma et al. [19] estimated the percentage of atomic CH mixed into the DT fuel in ICF experiments conducted at the NIF. The derived values typically range from approximately 0% to 5%. Therefore, we adopt $R = 0.001$, 0.01, and 0.05 in the following calculations. For the situation of Be mixing, $R = 0.05$ corresponds to an impurity mass fraction of 0.18. When the impurity is Au ions, the mass fraction becomes 0.80.

According to the average atom model [26], the total volume of the mixed plasma equals the sum of volumes occupied by its individual components. Moreover, from the condition of thermodynamic equilibrium under Fermi-Dirac statistics, the chemical potentials of all components in the mixture are equal. This suggests that the number densities of free electrons ionized by them are also equal. Based on the aforementioned conditions, the following relationships are derived for the case of Be mixing: $\frac{2.5+9R}{\rho_{\rm mix}} = \frac{2.5}{\rho_{\rm DT}} + \frac{9R}{\rho_{\rm Be}}$ and $\frac{\rho_{\rm DT}}{2.5} = \frac{\rho_{\rm Be}}{9} \cdot < Z_{\rm Be} >$, in which the mass number of Be ions is taken as 9. For the case of Au mixing, similar expressions can be established: $\frac{2.5+197R}{\rho_{\rm mix}} = \frac{2.5}{\rho_{\rm DT}} + \frac{197R}{\rho_{\rm Au}}$ and $\frac{\rho_{\rm DT}}{2.5} = \frac{\rho_{\rm Au}}{197} \cdot < Z_{\rm Au} >$, where 197 is the mass number of Au ions [22]. Thus, we can calculate the partial densities $\rho_{\rm DT}$ and $\rho_{\rm Be}$ (or $\rho_{\rm Au}$) at different $\rho_{\rm mix}$, $T_{\rm e}$ and R. The stopping power of each component can be further determined.

3. Calculation Methods and Properties of the Stopping Power

In this study, the stopping power is defined as: $\mathrm{SP} = \frac{\mathrm{d}E}{n_s \mathrm{d}x}$, where n_s denotes the number density of plasma species s, and $\mathrm{d}E$ the energy loss of the projectile when it moves a distance $\mathrm{d}x$ in plasmas due to collisions with particles of species s.

For Be and Au plasmas, the nuclear stopping power is calculated using the model developed by He and Wang [28]. Based on the binary collision theory [5,29] and employing the potential given by the average atom model [26], it accurately captures the negative nuclear stopping power that occurs when the projectile energy falls below the ion temperature. This model agrees well with the binary collision model that uses a corrected Coulomb logarithm in high-Z plasmas. For low-Z conditions, its results reduce to those given by the conventional binary collision model [5,28]. Throughout the considered temperature range, Be ions are treated as fully ionized, whereas Au ions are partially ionized at lower temperatures. Consequently, the electronic stopping power in the Be plasma only results from free electrons, while for the Au plasma it includes contributions from the impact excitation and ionization of bound electrons, along with their inverse processes. The stopping power caused by free electrons is evaluated using the quantum dielectric function [13], which introduces the Bose statistics to account for the projectile recoil effect. This approach ensures the end of heating when the projectile energy is lower than the electron temperature, and can well reproduce the results given by the recommended Jackson model [10,30]. For contributions from bound electrons, we adopt the model of He and Wang [10], which uses the first-order Born approximation based on the relativistic average atom model [27]. The derived cross sections show good agreement with results from solving the time-dependent Schrödinger equation over a wide range of projectile energies. This model also successfully explained the experimental energy loss data in partially ionized plasmas [31,32].

The calculated nuclear stopping power for Be and Au plasmas when $T_\mathrm{e} = 5.0$ keV and $T_\mathrm{i} > T_\mathrm{e}$ are shown in Figures 2a and 2b. The density is set to be 4.15 g/cm^3 as an example. The nuclear stopping power increases rapidly with the projectile energy E_p at low energies for all T_i. Then it reaches a peak and gradually decreases to near 0. As T_i increases, the peak height decreases, while the corresponding peak position shifts to higher E_p. When the projectile energy is sufficiently high (e.g., $E_\mathrm{p} \geq 100$ keV/u for Be and $E_\mathrm{p} \geq 50$ keV/u for Au), the nuclear stopping power curves at different T_i gradually converge and eventually coincide, becoming almost independent of T_i. This is because in this case the velocity of the projectile is much higher than that of the target ions. Henceforth such E_p range is referred to as the asymptotic region [22]. The electronic stopping power increases monotonically with E_p and shows no dependence on T_i, since the mass of electrons is too small compared with that of ions. The ionic component dominates the total stopping power only over a limited range of E_p. Its contribution diminishes as T_i increases. Under the circumstance of $T_\mathrm{i} = T_\mathrm{e}$, the nuclear stopping power is about 0 when the total projectile energy is comparable to T_e [22]. In the investigated two-temperature plasmas, this energy grows with T_i, and it is larger than the value when $T_\mathrm{i} = T_\mathrm{e} = 5.0$ keV. Compared to the nuclear stopping power in Be plasmas ($\mathrm{SP}_{\mathrm{Be-i}}$, Figure 2a), that in Au plasmas ($\mathrm{SP}_{\mathrm{Au-i}}$, Figure 2b) is larger due to the higher charge state of Au ions. Moreover, at the same T_i, the peak of $\mathrm{SP}_{\mathrm{Au-i}}$ corresponds to a lower E_p, which can be attributed to the smaller thermal velocity of Au ions. For the same reason, the E_p value at which $\mathrm{SP}_{\mathrm{Au-i}} = 0$ is also lower than that at which $\mathrm{SP}_{\mathrm{Be-i}} = 0$. For the case in which the density is 415.0 g/cm^3, the behaviors of relevant stopping powers are similar with those shown in Figures 2a-2b. However, since the

radius of the ion sphere where the average atom is enclosed becomes shorter, $\mathrm{SP_{Be-i}}$ and $\mathrm{SP_{Au-i}}$ are smaller at the same temperature. The electronic stopping powers ($\mathrm{SP_{Be-e}}$ and $\mathrm{SP_{Au-e}}$) are also smaller, because the screening from target electrons is stronger at higher number densities.

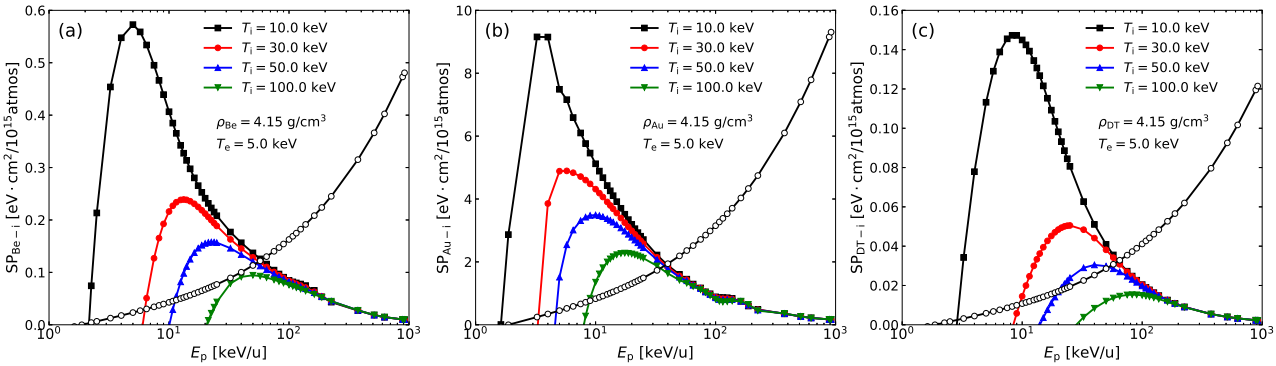


Fig. 2. (a) Nuclear stopping power $\mathrm{SP_{Be-i}}$ for α particles moving in Be plasmas varying with the projectile energy E_p, when $\rho_\mathrm{Be} = 4.15$ g/cm^3 and $T_\mathrm{e} = 5.0$ keV. The colors and symbols of curves mark different ion temperatures T_i. The curve with open circles represents electron stopping power $\mathrm{SP_{Be-e}}$. (b) Similar to (a) but for α particles moving in Au plasmas. (c) Similar to (a) but for α particles moving in DT plasmas.

For the DT plasma, the stopping power is calculated from the model proposed by He et al. [2]. It treats the plasma as an ion-electron two-component system to consistently incorporate the plasma polarization [33] and the projectile recoil [13]. Comparisons by He et al. [2] with the model proposed by Li and Petrasso [14] and the BPS model [15] demonstrate good agreement and reliable performance of this model for a wide range of plasma temperatures and densities.

The stopping power in the DT plasma exhibits similar characteristics to those discussed above, as shown in Figure 2c. Since DT ions are fully ionized, their electronic stopping power $\mathrm{SP_{DT-e}}$ is entirely contributed by free electrons. As for the nuclear stopping power $\mathrm{SP_{DT-i}}$, it also rises rapidly from 0 with increasing E_p, reaches a peak, and then gradually decreases toward near 0. At a fixed electron temperature, $\mathrm{SP_{DT-i}}$ decreases as T_i enhances, with its peak moving to higher E_p. When compared with $\mathrm{SP_{Be-i}}$ and $\mathrm{SP_{Au-i}}$, the peak in $\mathrm{SP_{DT-i}}$ is located at larger E_p under the same conditions, owing to the smaller mass and hence higher thermal velocity of DT ions. The $\mathrm{SP_{DT-i}}$ curves with various T_i enter the asymptotic region at high E_p as well. The value of $\mathrm{SP_{DT-i}}$ is smaller than $\mathrm{SP_{Be-i}}$ and $\mathrm{SP_{Au-i}}$, which results from the lower charge state of DT ions. Additionally, $\mathrm{SP_{Au-i}}/79.0$ is always smaller than $\mathrm{SP_{DT-i}}$. This is because the screening of the nuclear potential by electrons in the average-atom model weakens the interaction between the projectile and the target ion [22]. $\mathrm{SP_{Be-i}}/4.0$, however, can be either higher or lower than $\mathrm{SP_{DT-i}}$, which demonstrates that the electron screening in Be is less effective than that in Au. The fact that some $\mathrm{SP_{Be-i}}/4.0$ values exceed those of $\mathrm{SP_{DT-i}}$ may also be attributed to the different nuclear stopping power models applied to the impurity and DT ions in this study.

4. Electron-Ion Energy Partition in the Mixed Plasmas

Table 1. The energy partition fraction of DT ions, electrons and Be ions multiplied by 100, when $\rho_\mathrm{mix} = 4.15$ g/cm^3 and $T_\mathrm{i} > T_\mathrm{e}$. Here the symbols DT, e, and Be represent $100\eta_\mathrm{DT}$, $100\eta_\mathrm{e}$, and $100\eta_\mathrm{Be}$, respectively.

T_e [keV]	T_i [keV]	$R = 0.0$		$R = 0.001$			$R = 0.01$			$R = 0.05$		
		DT	e	DT	e	Be	DT	e	Be	DT	e	Be
1.0	5.0	3.54	96.3	3.53	96.3	0.01	3.42	96.3	0.13	2.99	96.3	0.55
	10.0	3.24	96.4	3.22	96.4	0.01	3.12	96.4	0.13	2.71	96.4	0.55
	30.0	2.32	96.7	2.31	96.7	0.01	2.23	96.6	0.11	1.93	96.6	0.47
	50.0	1.82	96.5	1.81	96.5	0.01	1.75	96.5	0.09	1.52	96.4	0.40
5.0	10.0	13.2	86.4	13.2	86.4	0.05	12.7	86.4	0.52	11.1	86.3	2.24
	30.0	12.1	86.8	12.1	86.8	0.05	11.7	86.8	0.53	10.1	86.6	2.27
	50.0	10.9	87.4	10.9	87.4	0.05	10.5	87.3	0.51	9.02	87.1	2.19
10.0	30.0	21.8	77.2	21.7	77.2	0.10	20.9	77.2	0.93	18.1	77.0	3.98
	50.0	20.6	77.7	20.5	77.7	0.10	19.8	77.6	0.94	17.0	77.3	3.98

Table 2. The energy partition fraction of DT ions, electrons and Au ions multiplied by 100, when $\rho_{\rm mix} = 4.15$ g/cm^3 and $T_i > T_e$. Here the symbols DT, e, and Au represent $100\eta_{\rm DT}$, $100\eta_e$, and $100\eta_{\rm Au}$, respectively.

T_e [keV]	T_i [keV]	$R = 0.0$		$R = 0.001$			$R = 0.01$			$R = 0.05$		
		DT	e	DT	e	Au	DT	e	Au	DT	e	Au
1.0	5.0	3.54	96.3	3.45	96.3	0.10	2.44	96.7	0.70	1.08	97.2	1.51
	10.0	3.24	96.4	3.04	96.3	0.09	2.10	96.7	0.65	0.89	97.2	1.37
	30.0	2.32	96.7	2.17	96.3	0.08	1.44	96.6	0.56	0.58	96.9	1.14
	50.0	1.82	96.5	1.71	96.4	0.08	1.13	96.5	0.52	0.45	96.7	1.05
5.0	10.0	13.2	86.4	12.4	86.5	0.56	8.20	87.6	3.64	3.34	88.8	7.28
	30.0	12.1	86.8	11.2	86.8	0.57	7.16	87.8	3.61	2.76	88.9	6.91
	50.0	10.9	87.4	10.2	87.4	0.60	6.32	88.2	3.66	2.37	89.1	6.74
10.0	30.0	21.8	77.2	20.2	77.4	1.03	13.1	78.9	6.59	5.14	80.6	12.8
	50.0	20.6	77.7	19.2	77.8	1.11	12.1	79.2	6.80	4.64	80.8	12.7

We now examine the effects of impurity mixing by calculating the electron-ion energy partition fractions in the two-temperature mixed plasmas. According to previous studies [2,22,34], the energy partition fractions for DT ions, electrons, and impurity ions can be defined as: $\eta_{\rm DT} = \frac{\int_{E_m}^{E_0} \tau_{\rm DT}(E_{\rm p}){\rm d}E_{\rm p}}{E_0}$, $\eta_{\rm e} = \frac{\int_{E_m}^{E_0} \tau_{\rm e}(E_{\rm p}){\rm d}E_{\rm p}}{E_0}$, and $\eta_{\rm IP} = \frac{\int_{E_m}^{E_0} \tau_{\rm IP}(E_{\rm p}){\rm d}E_{\rm p}}{E_0}$, in which IP represents Be or Au in this work. The integrands for the above equations are given by: $\tau_{\rm DT} = \frac{{\rm SP}_{\rm DT-i}}{({\rm SP}_{\rm DT-i}+{\rm SP}_{\rm DT-e})+R({\rm SP}_{\rm IP-i}+{\rm SP}_{\rm IP-e})}$, $\tau_{\rm e} = \frac{{\rm SP}_{\rm DT-e}+R\cdot{\rm SP}_{\rm IP-e}}{({\rm SP}_{\rm DT-i}+{\rm SP}_{\rm DT-e})+R({\rm SP}_{\rm IP-i}+{\rm SP}_{\rm IP-e})}$, and $\tau_{\rm IP} = \frac{R\cdot{\rm SP}_{\rm IP-i}}{({\rm SP}_{\rm DT-i}+{\rm SP}_{\rm DT-e})+R({\rm SP}_{\rm IP-i}+{\rm SP}_{\rm IP-e})}$. The upper integration limit, $E_0 = 885$ keV/u, corresponds to the birth energy of α particles in DT fusion. The lower limit E_m is the $E_{\rm p}$ at which α-heating ends, ensuring that all the stopping powers remain positive within the integration domain. For $R = 0$ and $R \to +\infty$, the definition of the energy partition fraction reduces to the cases of pure DT plasmas and pure impurity plasmas, respectively.

Based on the expressions above, we calculated the energy partition of α-heating in the mixtures when $T_i > T_e$. The results for Be-mixed and Au-mixed cases at $\rho_{\rm mix} = 4.15$ g/cm^3 are presented in Tables 1 and 2, respectively. For both cases, $\eta_{\rm DT}$ decreases with R for fixed T_e and T_i. In the DT-Be mixture, the decline is gradual within the range of $R \leq 0.01$. For the DT-Au mixture, this range is $R \leq 0.001$. A significant ($> 10\%$) drop in $\eta_{\rm DT}$ occurs as R takes larger values. In other words, the mixing of Be ions has a strong influence on $\eta_{\rm DT}$ when $R \geq 0.05$, while Au mixing does so at a lower concentration of $R \geq 0.01$. This difference is caused by the higher charge state and consequently greater stopping powers of Au ions relative to Be ions, as shown in Figures 2a-2b. The energy partition fractions of ions, including $\eta_{\rm DT}$, $\eta_{\rm Be}$ and $\eta_{\rm Au}$, rise up with T_e when both T_i and R

are fixed, due to the rapid decreasing of the electronic stopping powers with T_e. The sum of energy partition fractions in both Tables 1 and 2 is always smaller than 1. This is attributed to the fact that the heating stops when E_p falls to E_m, so the energy of α particles cannot be fully transferred to the target ions.

To investigate the tendency for η_{DT} to vary with T_i, we define the reduction percentage resulting from the impurity mixing as: $\beta = 1 - \frac{\eta_{DT}(R\neq 0)}{\eta_{DT}(R=0)}$. Figure 3 shows the calculated β at different T_e and R. All the curves in both cases share a similar shape, which indicates the dependence of β on T_i is almost unaffected by T_e and R. The β value in the DT-Be mixture remains around 0.04 at $R = 0.01$, while it varies between 0.15 and 0.18 at $R = 0.05$ (Figure 3a). In the case of Au mixing, β already reaches 0.3 to 0.4 at $R = 0.01$ and can exceed 0.7 with R increasing to 0.05 (Figure 3b). This characteristic is consistent with the behavior of η_{DT} presented in Tables 1 and 2, which is attributed to the distinct charge states of impurity ions.

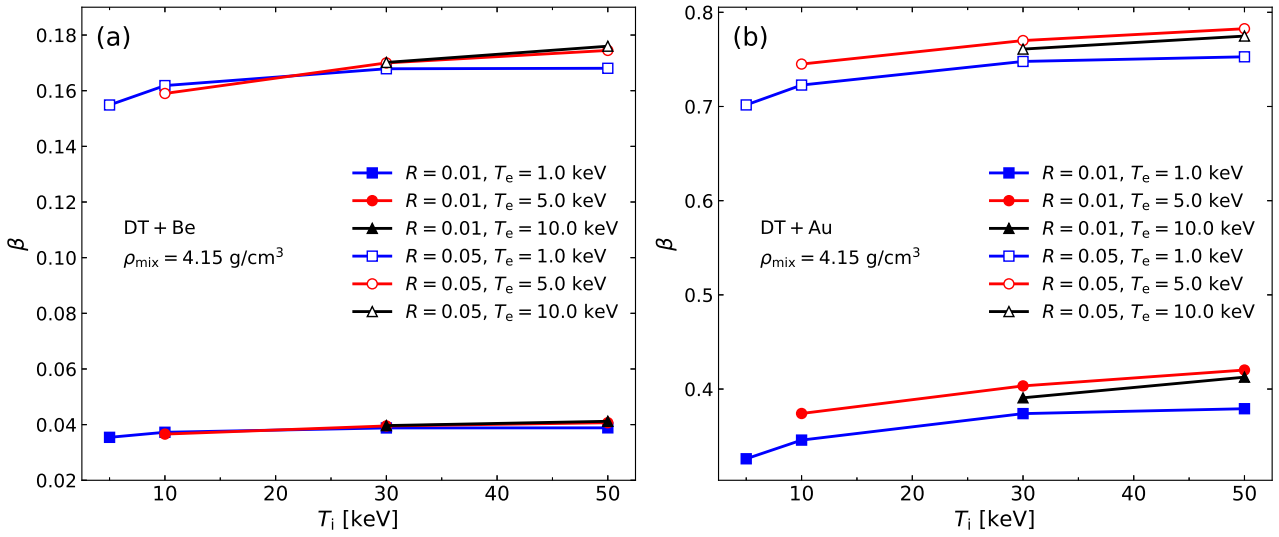


Fig. 3. (a) Parameter $\beta = 1 - \frac{\eta_{DT}(R\neq 0)}{\eta_{DT}(R=0)}$ varying with T_i in the case of Be mixing when $\rho_{mix} = 4.15$ g/cm^3. The curves with solid and empty symbols show the results of $R = 0.01$ and 0.05, respectively. The blue, red and black curves give the results when $T_e = 1.0$ keV, 5.0 keV and 10.0 keV, respectively. (b) Similar to (a) but in the case of Au mixing.

Parameter β in Figure 3 increases slowly in a narrow range along with the huge increasing of T_i at fixed T_e and R. To understand this behavior, we examine the integrand $\tau_{DT}(E_p)$ at different T_i when $\rho_{mix} = 4.15$ g/cm^3 and $T_e = 5.0$ keV (Figure 4). In both Be-mixed and Au-mixed cases, the value of τ_{DT} at $R = 0$ (no mixing) is larger than that at $R = 0.01$. The curves for two R values in Figure 4a show little difference, while a notable discrepancy is observed in Figure 4b. This also demonstrates that Au mixing already has a pronounced effect on the energy partition of DT ions at $R = 0.01$, but the influence of Be mixing remains limited under this condition. Figure 4 indicates that the E_p value contributing to the majority of the integral in the expression of η_{DT} lies within the range of $\sim$ 75 to 885 keV/u. Taking $R = 0.01$ as an example, the contribution from this energy range to η_{DT} at $T_i = 10.0$, 30.0, and 50.0 keV is about 58%, 63%, and 69% for the DT-Be mixture, whereas it is about 54%, 62%, and 69% for the DT-Au mixture. According to Figure 2, the stopping powers related to η_{DT} show little variation with T_i at fixed T_e over the range of $\sim$ 75 to 885 keV/u, which is close to the asymptotic region. Therefore, the τ_{DT} determining the majority of η_{DT} is almost independent of T_i. This appears as the coincidence of τ_{DT} curves across different T_i values over this energy range in Figure 4. As for the rest part of E_p, its contribution to η_{DT} under both $R = 0$ and $R = 0.01$ conditions varies synchronously with

T_i. Consequently, the changes from this part cancel each other out in the expression of β when T_i is altered. The aforementioned reasons together result in the observed weak dependence of β on T_i.

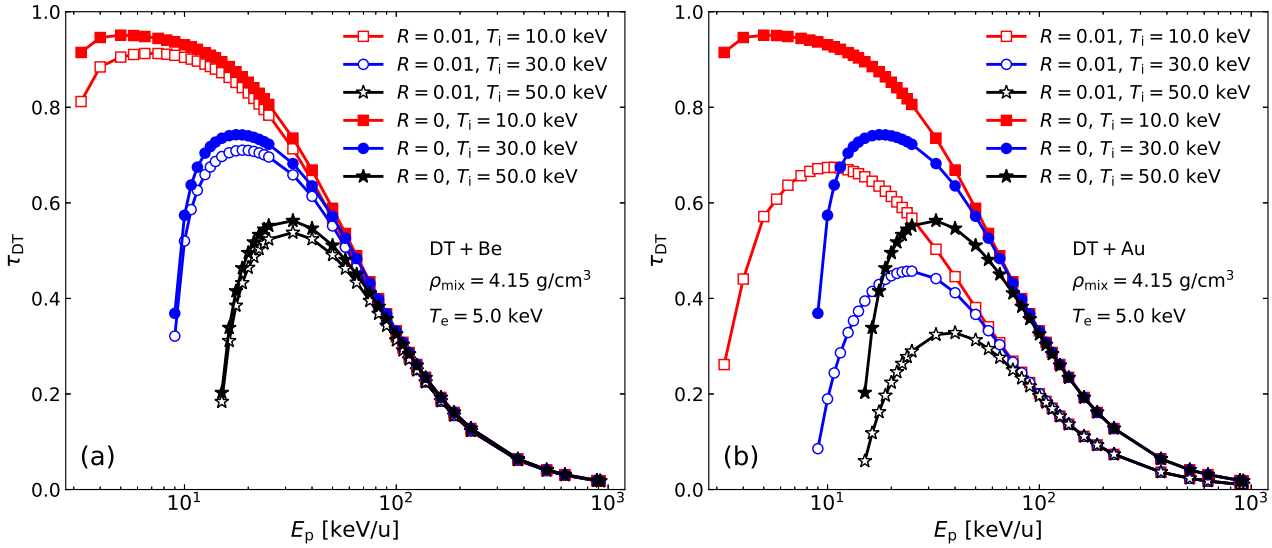


Fig. 4. (a) Parameter τ_DT varying with E_p in the case of Be mixing, when $\rho_\mathrm{mix} = 4.15$ g/cm^3 and $T_\mathrm{e} = 5.0$ keV. The curves with empty and solid symbols show the results of $R = 0.01$ and 0, respectively. The red, blue and black curves give the results of $T_\mathrm{i} = 10.0$ keV, 30.0 keV and 50.0 keV, respectively. (b) Similar to (a) but in the case of Au mixing.

We next focus on η_e in Tables 1 and 2. It can be seen that η_e is insensitive to T_i when T_e and R are fixed. The integrand $\tau_\mathrm{e}(E_\mathrm{p})$ at $\rho_\mathrm{mix} = 4.15$ g/cm^3, $T_\mathrm{e} = 5.0$ keV, and $R = 0.05$ is illustrated in Figure 5 to aid interpretation. For all values of T_i, the dominant contribution to η_e comes from the E_p range of ~ 100 to 885 keV/u. In the Be-mixed case, this part contributes 96%, 95%, 95%, and 95% of the integral at $T_\mathrm{i} = 10.0$, 30.0, 50.0, and 100.0 keV, respectively. For the Au-mixed case, the corresponding contribution is 95% at all given T_i. Figure 5 suggests that τ_e remains almost independent of T_i in this energy range. The reason responsible for this phenomenon is that, the nuclear stopping powers relevant to η_e calculation have entered their asymptotic regions according to Figure 2, while the electronic stopping powers do not depend on T_i. Therefore, the areas surrounded by different curves between ~ 100 and 885 keV/u in Figure 5 are almost equal, which dominates η_e in the entire range of E_p.

In Table 1, η_e shows little variation with R when T_e and T_i are fixed. However, Table 2 exhibits a gradual increase in η_e with R. To understand this difference, we also investigate how τ_e varies with R. Following the definition, $\tau_\mathrm{e} = \frac{1}{1+b(E_\mathrm{p},T_\mathrm{e},R)}$, in which parameter $b(E_\mathrm{p},T_\mathrm{e},R) = \frac{\mathrm{SP_{DT-i}}+\mathrm{R}\cdot\mathrm{SP_{IP-i}}}{\mathrm{SP_{DT-e}}+\mathrm{R}\cdot\mathrm{SP_{IP-e}}} = \frac{\mathrm{SP_{DT-i}}}{\mathrm{SP_{DT-e}}}\cdot\frac{1+(\mathrm{SP_{IP-i}}/\mathrm{SP_{DT-i}})R}{1+(\mathrm{SP_{IP-e}}/\mathrm{SP_{DT-e}})R}$ and IP $=$ Be, Au. Hence, the monotonic relationship between τ_e and R depends on the relative magnitude of coefficients $\mathrm{SP_{IP-i}}/\mathrm{SP_{DT-i}}$ and $\mathrm{SP_{IP-e}}/\mathrm{SP_{DT-e}}$. In the Be-mixed case, the two ratios are very close, which keeps $b(E_\mathrm{p},T_\mathrm{e},R)$ and τ_e nearly independent of R. For the DT-Au mixture, $\mathrm{SP_{Au-i}}/\mathrm{SP_{DT-i}}$ is smaller than $\mathrm{SP_{Au-e}}/\mathrm{SP_{DT-e}}$. This makes $b(E_\mathrm{p},T_\mathrm{e},R)$ decrease slowly with R rising, resulting in a gradual increase in τ_e and η_e.

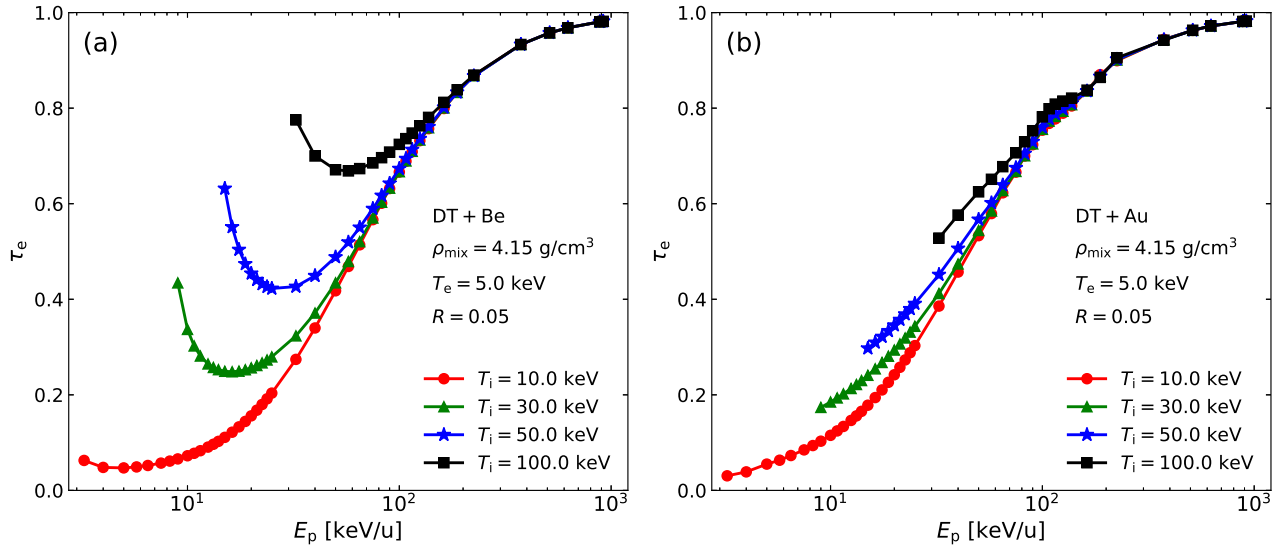


Fig. 5. (a) Parameter τ_e varying with E_p in the case of Be mixing, when $\rho_{mix} = 4.15$ g/cm^3, $T_e = 5.0$ keV, and $R = 0.05$. The colors and symbols of curves mark different T_i. (b) Similar to (a) but in the case of Au mixing.

The energy partition fraction of impurity ions is also insensitive to T_i when $T_e \geq 5.0$ keV, since all the related stopping powers enters their asymptotic regions in the energy range dominating the integral as discussed above. However, when $T_e = 1.0$ keV, η_{Be} decreases 31% and 27% with T_i varying from 5.0 to 50.0 keV when $R = 0.01$ and 0.05, while η_{Au} reduces 26% and 30%. We find that at low T_e, the E_p range over which nuclear stopping powers significantly affect the energy partition fractions becomes much narrower with increasing T_i. This makes η_{Be} and η_{Au} sensitive to T_i when $T_e = 1.0$ keV.

The results of $\rho_{mix} = 415.0$ g/cm^3 are also investigated. For the sake of briefness, we present the scopes for 100β to vary with T_i from the minimum value that satisfies $T_i > T_e$ to 50.0 keV at fixed T_e in Table 3. The data under two density conditions are close to each other, and their variations with R, T_e, and T_i are similar to those seen in Figure 3. For the Be-mixed case, 100β at $\rho_{mix} = 415.0$ g/cm^3 is nearly identical to that at $\rho_{mix} = 4.15$ g/cm^3. In contrast, for the Au-mixed case, the values at higher ρ_{mix} is slightly lower. As suggested by Figure 1, within the studied T_e range, $< Z_{Be} >$ is similar under both density conditions, whereas $< Z_{Au} >$ is significantly lower at the higher density. Thus, at $\rho_{mix} = 415.0$ g/cm^3, the lower charge state of Au ions gives rise to a smaller nuclear stopping power, which in turn causes a weaker reduction in η_{DT} and results in a lower β value.

We define a parameter $\gamma = \frac{\eta_{IP}}{\eta_{DT} R}$ to characterize the energy gained by each impurity ion compared to that by each DT ion on average during α-heating. Our calculations show that it is weakly dependent on R, which is consistent with the conclusion in the reference [22]. We give the scopes for γ to change with T_i at $R = 0.01$ in Table 3 as well. In the case of Be mixing, the γ value varies in a small range between 3.72 and 5.73. At fixed T_e, γ shows a slow enhancement with T_i. With increasing T_e, the scope of γ shifts, exhibiting a slightly raised lower limit and a reduced upper limit. In the Au-mixed case, γ is much larger, which also results from the higher charge state of Au ions. When $\rho_{mix} = 4.15$ g/cm^3 and $T_e = 1.0$ keV, γ changes from 29.0 to 47.0 as T_i increases from 5.0 to 50.0 keV. With T_e increasing to 5.0 and 10.0 keV, it rises further to the range of 45.0 to 56.0. When $\rho_{mix} = 415.0$ g/cm^3 is considered, the results are similar, except that γ takes a slightly lower value than under the low-density condition. The rise of γ with T_i is attributed to the earlier entry of SP_{IP-i} into its asymptotic region compared to SP_{DT-i}. This leads to a situation in which SP_{IP-i} changes very few

with T_i while $\mathrm{SP}_{\mathrm{DT-i}}$ falls with T_i. The disparity between asymptotic regions of $\mathrm{SP}_{\mathrm{Au-i}}$ and $\mathrm{SP}_{\mathrm{DT-i}}$ is more pronounced, which explains the steeper increase of γ with T_i in the DT-Au mixture. The increment of γ with T_e is driven by the increasing of $< Z_{\mathrm{Au}} >$ in hot plasmas, while its suppression at higher ρ_{mix} is again caused by the lower $< Z_{\mathrm{Au}} >$ under the dense condition.

Table 3. Scopes for 100β and $\gamma = \frac{\eta_{\mathrm{IP}}}{\eta_{\mathrm{DT}} R}$ (IP = Be, Au) to vary with T_i from the minimum value satisfying $T_\mathrm{i} > T_\mathrm{e}$ to 50.0 keV, at $T_\mathrm{e} = 1.0$, 5.0, and 10.0 keV for $\rho_{\mathrm{mix}} = 4.15$ g/cm^3 and 415.0 g/cm^3. For 100β the values at $R = 0.01$ and 0.05 are shown, while for γ the values at $R = 0.01$ are presented.

Be Mixing							
ρ_{mix} [g/cm^3]		4.15			415.0		
T_e [keV]		1.0	5.0	10.0	1.0	5.0	10.0
100β	$R = 0.01$	$3.54 \sim 3.88$	$3.66 \sim 4.07$	$3.97 \sim 4.12$	$3.42 \sim 3.91$	$3.66 \sim 4.08$	$4.00 \sim 4.16$
	$R = 0.05$	$15.5 \sim 16.8$	$15.9 \sim 17.4$	$17.0 \sim 17.6$	$15.0 \sim 16.9$	$15.9 \sim 17.5$	$17.2 \sim 17.8$
γ $[R = 0.01]$		$3.72 \sim 5.32$	$4.07 \sim 4.89$	$4.45 \sim 4.73$	$4.11 \sim 5.73$	$4.35 \sim 5.09$	$4.73 \sim 4.99$
Au Mixing							
ρ_{mix} [g/cm^3]		4.15			415.0		
T_e [keV]		1.0	5.0	10.0	1.0	5.0	10.0
100β	$R = 0.01$	$32.6 \sim 37.9$	$37.4 \sim 42.0$	$39.1 \sim 41.3$	$29.5 \sim 37.9$	$34.4 \sim 39.8$	$38.0 \sim 39.6$
	$R = 0.05$	$70.2 \sim 75.3$	$74.5 \sim 78.3$	$76.1 \sim 77.5$	$66.4 \sim 75.3$	$71.3 \sim 76.1$	$74.7 \sim 76.1$
γ $[R = 0.01]$		$29.0 \sim 47.0$	$45.0 \sim 48.0$	$50.0 \sim 56.0$	$27.0 \sim 44.0$	$43.0 \sim 49.0$	$46.0 \sim 51.0$

5. Conclusions

In this study, we investigate the influence of impurity mixing with ICF DT plasmas on α-heating when the ion temperature is higher than the electron temperature ($T_\mathrm{i} > T_\mathrm{e}$), by calculating the electron-ion energy partition in the mixtures. Two kinds of impurity ions, Be and Au, are considered, which are taken as examples of low-Z and high-Z materials, respectively. We study two mixture densities of 4.15 and 415.0 g/cm^3, which correspond to ion number densities of 10^{24} and 10^{26} cm^{-3} in pure DT plasmas, respectively. T_e ranges from 0.1 to 100.0 keV in our work. The partial densities of DT and impurity ions in the mixture are derived under thermodynamic equilibrium using the average atom model. The nuclear stopping power in the impurity plasma is calculated using the binary collision model based on the average atom model potential [28]. The stopping power contributed by free electrons is obtained through the quantum dielectric function that includes the projectile recoil effect [13]. The contribution from bound electrons is computed via the first-order Born approximation based on the relativistic average atom model [10,27]. We apply the model developed by He et al. [2] to calculate stopping powers in DT fuels, which combines the projectile recoil and the plasma polarization together in electron-ion two-component plasmas. The results are summarized as follows.

1. When the degree of mixing (R) reaches 0.05, Be mixing reduces the energy partition fraction of DT ions (η_{DT}) by approximately 15% to 18%, while Au mixing can induce a drop exceeding 30% even at $R = 0.01$.

2. The reduction percentage of η_{DT} increases slowly with T_i at fixed T_e and R. Meanwhile, its dependence on T_i is insensitive to T_e and R.

3. The energy partition fraction of electrons is independent of T_i for fixed T_e and R. Besides, it varies weakly with R in the Be-mixed case, while a gradual increase with R is observed in the Au-mixed case.

4. The energy partition fraction of impurity ions decreases with T_i at $T_\mathrm{e} = 1.0$ keV, but its variation becomes much smaller at higher T_e.

5. The relative energy gain of each Au ion over each DT ion on average is greater than that of a Be ion, and this ratio increases slowly with T_i at fixed T_e.

We have evaluated the extent of the impact of different impurities under two-temperature conditions based on the calculation results, which suggest that Au mixing is more harmful to the self-sustained burning in ICF than Be mixing, especially at high ion temperatures. Moreover, when ions are hotter, the energy partition for the DT fuel becomes smaller at a fixed electron temperature. The different charge states of ions lead to the fact that Au ions are heated more readily by α particles than Be ions, and Be ions more so than DT ions. This differential heating could result in temperature differences among the plasma species, which would be the topic of our next study. It should be noted that, in this work we only compute the stopping powers and energy partition in mixed plasmas under the assumption of equal ion temperatures, but we do not model the subsequent species-dependent temperature evolution arising from different energy gains.

The usage of the average atom model do not affect the conclusions of this work. The average ionization degrees of Be and Au ions are governed by the electron temperature, and the interactions between ion spheres neglected by the model have minor influences on the calculations. We previously applied the same model to compute the average ionization degree in solid-density Be plasmas [32], and the results agreed well with experimental measurements. Besides, the ionization degree mainly affects the bound electron stopping power in the investigated mixture system, which has limited influences on the calculation of energy partition fractions. We also employed the same model to calculate stopping powers in partially ionized Aluminum plasmas [31] and solid-density Be plasmas [32]. The results again showed good agreement with experiments, which indicates that the uncertainties associated with the choice of the atomic model are negligible. In addition, several stopping power models over a broad range of density, temperature, ionization state, and atomic number are combined in our calculations. For the investigated hot dense DT plasmas, the recoil effect of the projectile and the polarization effect between DT ions and electrons are non-negligible. We adopt the dielectric model based on the two-component plasma [2], which can better handle the aforementioned effects. For the impurity ions, their charge states are significantly higher than those of DT ions (especially for Au ions), which leads to stronger coupling with the incident α particles. In such cases, the BPS model and the dielectric model, both of which are based on perturbation theory, are no longer applicable. Therefore, we choose the binary collision model based on the non-perturbative approach [28] to compute the nuclear stopping power of impurity ions. For the free electrons in the impurity plasmas which have low charge states, we describe their stopping power using a dielectric formalism similar to that for the DT plasmas [13]. For the partially ionized dense Au plasmas, we use the first-order Born approximation [10] based on the relativistic average atom model [27] to calculate the stopping power due to inelastic collisions with bound electrons. In strongly coupled and degenerate dense plasmas, the average atom model provides a good description of the screened Coulomb interaction potential. Moreover, this model allows a detailed treatment of atomic processes in the plasma. As mentioned before, the

results given by our model agreed well with experiments [31,32]. The above discussions validate that our models are suitable for addressing the hot dense mixed plasmas considered in this study. A limitation of our current models is the reduced accuracy for the inelastic collision stopping power at low and intermediate projectile energies, which arises from the usage of the first-order Born approximation. The development of high-order Born approximation methods is needed in future work to achieve better accuracy in this regime.

In the calculation of energy partition fractions in mixed plasmas, we combine the stopping contributions of DT and impurity components using their separately calculated stopping powers. We believe that the effect of mixing on the calculation of stopping powers is relatively weak through qualitative analysis. According to our calculations using the average atom model based on single element and comparisons with experimental results [10,31,32], the primary factors affecting stopping powers are the plasma temperature, density, and the corresponding average ionization degree, while the influences of electron correlation and atom correlation are negligible. Besides, the dominant contribution of the energy partition fraction arises from the free electron stopping power. The correlation effects induced by mixing do not alter the final outcomes. Therefore, we conclude that for mixed plasmas, despite the changes in electron response and inter-species correlations introduced by mixing, these effects are not dominant factors affecting the stopping powers, and their impact on the energy partition results is minor. Although we are unable to quantitatively assess the influence of mixing-induced correlation effects on stopping powers currently, density functional theory [35] may offer a viable approach. However, the substantial computational cost makes this method challenging. To the best of our knowledge, no such study has been reported to date. The findings of this study offer insights for future investigations on the temperature relaxation process in hot dense plasmas. They also contribute to the accurate modeling of controlled fusion and provide practical references for ICF ignition target design.

Data availability statement

The data that support the findings of this study are available from the corresponding author upon reasonable request.

Acknowledgment

The authors thank Prof. Xiang Gao, Prof. Cheng-Liang Lin, Prof. Rui Jin, and Prof. Xiao-Qing Hu for beneficial discussions. This work was supported by the National Key Research and Development Program of China No. 2022YFA1602500, the National Natural Science Foundation of China Nos. 12274039, U2430208, and the China Postdoctoral Science Foundation Nos. 2026M794841, GZC20260201.

References

[1] D'Avanzo J, Lontano M, Tome' E and Bortignon P 1995 *Nucl. Fusion* **35** 210

[2] He B, Wang Z G and Wang J G 2018 *Phys. Plasmas* **25** 012704

[3] Bohr N 1913 *Phil. Mag.* **25** 10–31

[4] Bohr N 1915 *Phil. Mag.* **30** 581–612

[5] Butler S T and Buckingham M J 1962 *Phys. Rev.* **126**(1) 1–4

[6] Bethe H 1930 *Ann. Phys.* **397** 325–400

[7] Bethe H 1932 *Z. Physik* **76** 293–299

[8] Bloch F 1933 *Ann. Phys.* **408** 285–320

[9] Bloch F 1933 *Z. Physik* **81** 363–376

[10] He B and Wang J G 2013 *Nucl. Fusion* **53** 093009

[11] Lindhard J 1954 *Dan. Mat. Fys. Medd.* **28**

[12] Sigmar D and Joyce G 1971 *Nucl. Fusion* **11** 447

[13] Arista N R and Brandt W 1981 *Phys. Rev. A* **23**(4) 1898–1905

[14] Li C K and Petrasso R D 1993 *Phys. Rev. Lett.* **70**(20) 3059–3062

[15] Brown L S, Preston D L and Singleton Jr R L 2005 *Phys. Rep.* **410** 237–333

[16] Lindl J D, Amendt P, Berger R L, Glendinning S G, Glenzer S H, Haan S W, Kauffman R L, Landen O L and Suter L J 2004 *Phys. Plasmas* **11** 339–491

[17] Amendt P, Colvin J D, Tipton R E, Hinkel D E, Edwards M J, Landen O L, Ramshaw J D, Suter L J, Varnum W S and Watt R G 2002 *Phys. Plasmas* **9** 2221–2233

[18] Gus'kov S, Il'in D and Sherman V 2011 *Plasma Phys. Rep.* **37** 1020–1034

[19] Ma T, Patel P K, Izumi N, Springer P T, Key M H, Atherton L J, Benedetti L R, Bradley D K, Callahan D A, Celliers P M, Cerjan C J, Clark D S, Dewald E L, Dixit S N, Döppner T, Edgell D H, Epstein R, Glenn S, Grim G, Haan S W, Hammel B A, Hicks D, Hsing W W, Jones O S, Khan S F, Kilkenny J D, Kline J L, Kyrala G A, Landen O L, Le Pape S, MacGowan B J, Mackinnon A J, MacPhee A G, Meezan N B, Moody J D, Pak A, Parham T, Park H S, Ralph J E, Regan S P, Remington B A, Robey H F, Ross J S, Spears B K, Smalyuk V, Suter L J, Tommasini R, Town R P, Weber S V, Lindl J D, Edwards M J, Glenzer S H and Moses E I 2013 *Phys. Rev. Lett.* **111**(8) 085004

[20] Wang Z, Fu Z G, He B and Zhang P 2014 *Phys. Plasmas* **21** 072703

[21] Wang Z, Fu Z G and Zhang P 2014 *Phys. Plasmas* **21** 102307

[22] He B and Wang J G 2023 *Contrib. Plasma Phys.* **63** e202300042

[23] Lin W, Zhang H, He B, Cai H and Zhu S 2024 *Phys. Plasmas* **31** 122702

[24] Adrian P J, Florido R, Grabowski P E, Mancini R, Bachmann B, Benedict L X, Johnson M G, Kabadi N, Lahmann B, Li C K, Petrasso R D, Rinderknecht H G, Regan S P, Séguin F H, Singleton R L, Sio H, Sutcliffe G D, Whitley H D and Frenje J A 2022 *Phys. Rev. E* **106**(5) L053201

[25] van de Wetering J J, Angus J R, Farmer W, Geyko V, Ghosh D, Grote D, Weber C and Zimmerman G 2025 *Phys. Rev. E* **112**(4) 045207

[26] Nikiforov A F, Novikov V G and Uvarov V 2005 *Quantum-Statistical Models of Hot Dense Matter: Methods for Computation Opacity and Equation of State* (Basel: Birkhäuser Basel) chap The Hartree-Fock-Slater model for the average atom, pp 107–141 ISBN 978-3-7643-7346-7

[27] Rozsnyai B F 1972 *Phys. Rev. A* **5**(3) 1137–1149

[28] He B and Wang J G 2015 *High Energy Density Phys.* **17** 248–253

[29] Faussurier G, Blancard C and Gauthier M 2013 *Phys. Plasmas* **20** 012705

[30] Mehlhorn T A 1981 *J. Appl. Phys.* **52** 6522–6532

[31] He B and Wang J G 2014 *Phys. Plasmas* **21** 063111

[32] He B, Meng X J, Wang Z G and Wang J G 2017 *Phys. Plasmas* **24** 033110

[33] Skupsky S 1977 *Phys. Rev. A* **16**(2) 727–731

[34] Brown L S, Preston D L and Singleton Jr R L 2012 *Phys. Rev. E* **86**(1) 016406

[35] Echenique P M, Nieminen R M, Ashley J C and Ritchie R H 1986 *Phys. Rev. A* **33**(2) 897–904